



HAL
open science

New Physics-Based Turbocharger Data-Maps Extrapolation Algorithms: Validation on a Spark-Ignited Engine

Jamil El Hedef, Guillaume Colin, Vincent Talon, Yann Chamaillard

► **To cite this version:**

Jamil El Hedef, Guillaume Colin, Vincent Talon, Yann Chamaillard. New Physics-Based Turbocharger Data-Maps Extrapolation Algorithms: Validation on a Spark-Ignited Engine. 2012 IFAC Workshop on Engine and Powertrain Control, Simulation and Modeling (ECOSM), Oct 2012, Rueil-Malmaison, France. hal-00767727v1

HAL Id: hal-00767727

<https://hal.science/hal-00767727v1>

Submitted on 20 Dec 2012 (v1), last revised 7 Jan 2013 (v2)

HAL is a multi-disciplinary open access archive for the deposit and dissemination of scientific research documents, whether they are published or not. The documents may come from teaching and research institutions in France or abroad, or from public or private research centers.

L'archive ouverte pluridisciplinaire **HAL**, est destinée au dépôt et à la diffusion de documents scientifiques de niveau recherche, publiés ou non, émanant des établissements d'enseignement et de recherche français ou étrangers, des laboratoires publics ou privés.

New Physics-Based Turbocharger Data-Maps Extrapolation Algorithms: Validation on a Spark-Ignited Engine

J. El Hadeif *, G. Colin*, V.Talon**, Y.Chamaillard*

*Laboratoire PRISME, 8 rue Léonard de Vinci, 45000 Orléans cédex 2, FRANCE (Tel: +33238494383; e-mail: jamil.el-hadeif@etu.univ-orleans.fr).

** Renault SA - CTL, 1 Allée de Cornuel, 91510 Lardy, FRANCE (Tel: +33611527597; e-mail: vincent.talon@renault.com)

Abstract: Objectives in terms of pollutant emissions and fuel consumption reduction, as well as development costs and time to market reduction, has led car manufacturers to use more and more system simulation. However, among all the fields in which it has enabled to achieve these goals, the control development stage is one of those, in which major improvements can still be achieved. In this context and with the increasing penetration of downsized engines, turbocharger modeling has become one of the biggest challenges in engine simulation. This paper focus on the validation of compressor and turbine data maps, extrapolated using new physics-based extrapolation algorithms. The study led to excellent prediction performances for two classical control-oriented models. Conclusions stress: 1- The improvement of the extrapolation robustness, in particular in the low turbocharger rotational speeds zone. 2- The possibility to keep a low calculation time as well as maintaining the same calibration effort.

Keywords: Turbocharger, data-maps, interpolation, extrapolation, validation, transients, steady-state.

1. INTRODUCTION

Always more drastic pollutant emission standards constrained the car manufacturers to reduce the fuel consumption and pollutant emissions of internal combustion engines. This can be achieved by reducing the engine displacement as well as adding a turbocharger to the air path in order to maintain the same driving performances. In this context, model-based development strategies are a very promising way to deal with this increasing complication of engines technical definition (Gissinger et al., (2002), Dauron, (2007), Guzzella et al., (2004)). In fact, model-based development strategies such as validation on virtual test bench as well as model-embedded control are now widely integrated in car manufacturers' development processes and research programs.

In the case of turbocharged engines, the turbocharger sub-model accuracy represents the biggest challenge. Usually, for calculation time considerations, it relies on extrapolated manufacturer's data maps. The goal of this study is to confirm that new physics-based extrapolation algorithms (El Hadeif et al., (2012)) implemented in classical zero dimension engine models (usually implemented using commercial software or in any programming language) lead to accurate results, without increasing the calibration effort. The results for two different models are presented in this paper: first, a reference simulator implemented using the commercial software LMS AMESim, then, a Matlab code designed to be embedded in a control law.

2. ENGINE TECHNICAL DEFINITION

The work is based on a multi-points injection 1.2L turbocharged spark-ignited engine (see figure 1). Such a *light* technical definition increases the turbocharger importance.

As a consequence, it makes possible to estimate the benefit induced by the new data-maps in control-oriented models.

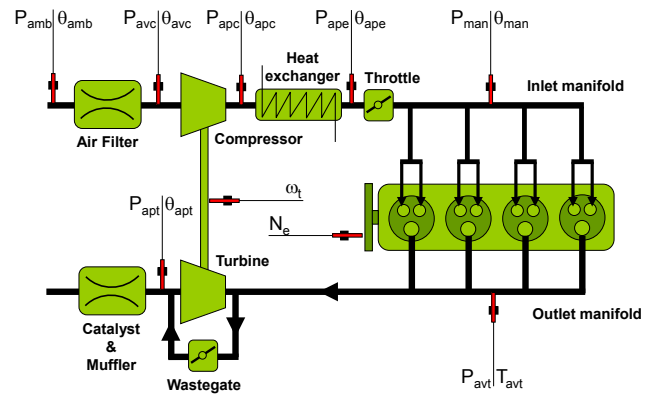


Fig. 1. Engine and sensors configuration used for the study. The engine is a turbocharged four-cylinder spark-ignited engine. Actuators actual position is also recorded.

Injection and throttle command and response have been recorded. The wastegate actual position could not be measured on the engine available for the study.

Pressure and temperature before and after each air path component have been acquired. The engine rotational speed and torque as well as the turbocharger rotational speed have also been measured.

3. REFERENCE SIMULATOR

A 0D mean value model has been developed to be used as a virtual test bench for the control development stage. Most of the components are taken from the IFP engine library. The

others are part of the mechanical and signal AMESim library, included in the standard package.

This model has been validated in steady state conditions as well as for transients. As such, it can be used to validate the control law using, for example, *hardware in the loop* testing.

3.1 Mean value engine model

A mean value engine model component provides the air mass flow rate, the engine torque, the friction torque and the energy given to the exhaust. All these outputs are estimated from data-maps which can be determined from the physical quantities available for the study (see figure 1).

This sub-model can be pre-validated by setting inlet and outlet manifold pressures, the inlet manifold temperature, the air-fuel ratio and the engine speed. In those conditions, the sub-model must already provide the right flow rate, torque and outlet manifold temperature.

3.2 Air path calibration

The air path of the model contains component sub-models for the air filter, the catalyst and the muffler. They are all based on a flow restriction model. The effective cross section parameter is calibrated to match the test bench data points.

For the throttle and the wastegate, a flow restriction model is also used. In the first case, the effective area is known for every position of the actuator. For the wastegate, a PID controller determines the effective area which matches the inlet manifold pressure.

The heat exchanger is modelled as the combination of a standard heat exchanger and a flow restriction. The first one is set to match the inlet manifold temperature test bench data points. The second one is calibrated to match the pressure drop measured on the test bench (see figure 1).

The compressor and turbine models both rely on data-maps for pressure ratio, flow rate and efficiency. These data-maps are extrapolated from manufacturer's steady state data points. An innovative physical-based extrapolation strategy has been developed and is presented in section 5 (El Hadeif et al., (2012)).

Compressor and turbine models are mechanically linked by a shaft which inertia is supposed to be known.

4. CONTROL EMBEDDED MODEL

A control embedded model must combine accuracy and stability while keeping a low calculation time. In this case, a 0D approach combined with a mean value cylinders model usually appears to be the most appropriate (Moulin et al., (2008)). The model described below is a four-state 0D model which has been validated on steady state operations as well as on transients.

4.1 Air path discretization

The strategy used here discretizes the pipes into control volumes (see figure 2). Each of them represents a state of the model and as such, its dynamic is governed by a differential

equation. Between each of them, an orifice (usually a flow restriction) controls the flow rate at the inlet (respectively at the outlet) of the control volume (see figure 2).

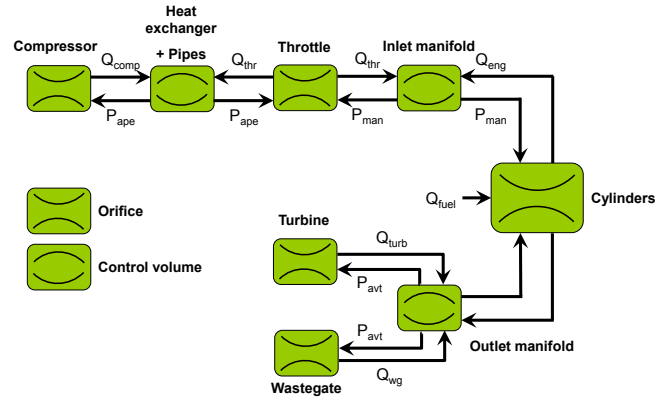


Fig. 2. Air path discretization: control volumes and restrictions.

In this model, the throttle and the wastegate are treated as flow restriction, while a data-map based model is used for the compressor and the turbine. In order to validate it, the same innovative data-maps construction as for the reference simulator is used here and detailed in section 5.

4.2 Reservoir model

In each control volume, Euler's mass, energy and momentum equations are applied:

$$\frac{\partial m}{\partial t} = Q_{m_{in}} - Q_{m_{out}} \quad (1)$$

$$\frac{\partial E}{\partial t} = Q_{m_{in}} \left(h_{in} + \frac{1}{2} v_{in}^2 \right) - Q_{m_{out}} \left(h_{out} + \frac{1}{2} v_{out}^2 \right) \quad (2)$$

$$\frac{\partial mv}{\partial t} = A(P_{in} + \rho_{in} v_{in}^2) - A(P_{out} + \rho_{out} v_{out}^2) \quad (3)$$

where m is the mass, E the energy, v the flow speed, Q_m the mass flow rate, h the enthalpy, A the cross section, P the pressure and ρ the fluid density. Indices "in" and "out" respectively stand for inlet and outlet of the considered control volume.

Neglecting the kinetic energy in the energy (2) and the ρv^2 term in the momentum (3), the enthalpy flow can be deduced:

$$Q_h = Q_m C_p \theta \quad (4)$$

where Q_h is the enthalpy flow, C_p the specific heat at constant pressure and θ the temperature.

It leads to the derivative of the internal energy U :

$$\frac{\partial U}{\partial t} = Q_{m_{in}} C_{p_{in}} \theta_{in} - Q_{m_{out}} C_{p_{out}} \theta_{out} \quad (5)$$

where U is the internal energy.

In a given volume V , it is directly linked to the pressure derivative:

$$\frac{\partial P}{\partial t} = \frac{\gamma - 1}{v} \frac{\partial U}{\partial t} \quad (6)$$

where γ is the ratio of specific heats.

Under the assumption of constant temperature in the reservoir (Hendricks, (2001)), only one state equation governs the dynamic of the control volume. It is given in Martin et al., (2009b) by:

$$\frac{\partial P}{\partial t} = \frac{\gamma r}{V} (Q_{min} \theta_{in} - Q_{mout} \theta_{out}) \quad (7)$$

where r is the fluid gas constant.

The specific heat at constant pressure must then be defined as

$$C_p = \frac{\gamma r}{\gamma - 1} \quad (8)$$

As described in figure 2, the model contains three control volumes: the heat exchanger, the inlet manifold and the outlet manifold. In each of them, the pressure dynamic is computed using (7).

4.3 Orifice models

Inlet and outlet flow rates of control volumes are controlled by the orifices which separate them. For the throttle and the wastegate, a flow restriction model is used (Moulin et al., (2008)).

The flow is supposed to be compressible and isentropic. Under this hypothesis, the flow can be estimated using the pressure upstream and downstream the orifice (Heywood, (1988), Talon, (2004)):

$$\begin{cases} Q_m = \frac{P_{us}}{\sqrt{r T_{us}}} S_{eff} \sqrt{\gamma} \left(\frac{2}{\gamma+1}\right)^{\frac{\gamma+1}{2(\gamma-1)}} & \text{if } \frac{P_{ds}}{P_{us}} \geq \left(\frac{2}{\gamma+1}\right)^{\frac{\gamma}{\gamma-1}} \\ Q_m = \frac{P_{us}}{\sqrt{r T_{us}}} S_{eff} \left(\frac{P_{ds}}{P_{us}}\right)^{\frac{1}{\gamma}} \sqrt{\frac{2\gamma}{\gamma-1} \left(1 - \left(\frac{P_{ds}}{P_{us}}\right)^{\frac{\gamma-1}{\gamma}}\right)} & \text{otherwise} \end{cases} \quad (9)$$

where S_{eff} is the effective area of the orifice. The indices "us" and "ds" respectively stand for upstream and downstream.

4.4 Temperatures

To establish (7), a constant temperature hypothesis has been done. This is the result of the fact that the dynamic of the temperature is considered to be slower than the pressure one. One can then consider:

$$\frac{\partial \theta}{\partial t} = 0 \quad (10)$$

As a result, the temperature in each reservoir can be computed algebraically. Many models exist in literature and depend of the considered volume. The one chosen here will be detailed on a case-by-case basis in the next sub-sections.

4.5 Compressor model

The compressor is considered in the model as a flow rate source. The flow rate is read in a data-map f_1 provided by the manufacturer and extrapolated as detailed in section 5:

$$Q_{comp} = f_1(\pi_{comp}, \omega_t) \quad (11)$$

where Q_{comp} is the compressor outlet mass flow rate, π_{comp} the compression ratio and ω_t the turbocharger rotational speed. f_1 is the extrapolated data-map.

The flow rate is distributed at a given temperature which depends of the compressor isentropic efficiency. It is compute algebraically using:

$$\theta_{apc} = \theta_{amb} \left(\frac{\pi_{comp}^{\frac{\gamma-1}{\gamma}} - 1}{\eta_{comp}} + 1 \right) \quad (12)$$

where θ_{apc} is the temperature downstream the compressor, θ_{amb} the atmospheric temperature and η_{comp} the compressor isentropic efficiency.

The isentropic efficiency of the compressor is read in a second data-map, also extrapolated from manufacturer's data:

$$\eta_{comp} = f_2(Q_{comp}, \omega_t) \quad (13)$$

where f_2 is the extrapolated data-map.

4.6 Turbine model

The turbine is modelled as a flow restriction which flow rate is directly read from a data-map:

$$Q_{turb} = f_3(\pi_{turb}, \omega_t) \quad (14)$$

where Q_{turb} is the turbine flow rate and π_{turb} the expansion ratio. f_3 is an extrapolated data-map.

The temperature of the flow at the outlet of the turbine can be obtained from the turbine isentropic efficiency:

$$\theta_{turb} = \theta_{avt} \left[1 - \eta_{turb} \left(1 - \left(\frac{1}{\pi_{turb}} \right)^{\frac{\gamma-1}{\gamma}} \right) \right] \quad (15)$$

where θ_{turb} is the turbine outlet temperature, θ_{avt} the outlet manifold temperature and η_{turb} the turbine isentropic efficiency.

As for the compressor, the turbine isentropic efficiency is read in a data-map f_4 :

$$\eta_{turb} = f_4(\pi_{turb}, \omega_t) \quad (16)$$

4.7 Mechanical turbocharger model

The particularity of the compressor and the turbine, as flow sources, is that they are mechanically linked. Neglecting frictions, the dynamical behaviour of the turbocharger is given by a fourth state equation which complete the model (Chauvin et al., (2011), Moulin et al., (2008)):

$$\dot{\omega}_t = \frac{1}{J} (T_{qturb} - T_{qcomp}) \quad (17)$$

where J is the turbocharger inertia, T_{qturb} and T_{qcomp} respectively represent the turbine and compressor torques.

Compressor and turbines torques are computed using the model described above. In both cases, they depend on the mass flow rate, the inlet and outlet temperature and the turbocharger rotational speed:

$$T_{qcomp} = \frac{Q_{comp} \times C_p \times (\theta_{apc} - \theta_{amb})}{\omega_t} \quad (18)$$

$$T_{qturb} = \frac{Q_{turb} \times C_p \times (\theta_{avt} - \theta_{turb})}{\omega_t} \quad (19)$$

4.8 Mass flow rate and volumetric efficiency

The flow rate Q_{eng} is defined as a function of the inlet manifold pressure and temperature as well as the engine speed (Heywood, (1988), Moulin et al., (2008)):

$$Q_{eng} = \frac{P_{man} V_{cyl} N_e}{r \theta_{man} 120} \times \eta_{vol} \quad (20)$$

where Q_{eng} is the engine flow rate, P_{man} and θ_{man} the manifold pressure and temperature, V_{cyl} the engine displacement, N_e the engine rotational speed and η_{vol} the volumetric efficiency.

The strategy consists to first calculate the theoretical mass flow rate at inlet manifold conditions, under the hypothesis of a perfect gas. This quantity is then multiplied by the volumetric efficiency η_{vol} which represents the ability of the engine to aspire this quantity of air from the manifold.

This ability directly depends from the geometry of the engine and the operating points:

$$\eta_{vol} = f_5 \left(N_e, \frac{P_{man}}{T_{man}} \right) \quad (21)$$

where f_5 is a second order polynomial calibrated on the steady state test bench measurements (average relative error is 1.7% with a standard deviation of 1.4% while maximum relative error is 8.9%).

4.9 Exhaust mass flow rate

At the outlet of the cylinders, the flow rate is the sum of the inlet mass flow rate described above and the fuel mass flow rate. The last one, if not known, can be computed using the air-fuel ratio AFR:

$$Q_{fuel} = Q_{eng} \times \frac{AFR}{14.7} \quad (22)$$

where Q_{fuel} is the fuel mass flow rate and AFR the air-fuel ratio.

4.10 Exhaust enthalpy flow rate and exhaust temperature

As underlined in Eriksson, (2007), when considering turbocharged engines, the exhaust enthalpy flow rate is essential. In fact, it represents the potential power that can be recovered by the turbine and as such, influences the intake air charge.

The outlet manifold temperature is computed using the inlet gas conditions (mass flow rate and temperature) and the fuel mass flow rate:

$$\theta_{avt} = \theta_{man} + k_{ech} \frac{Q_{fuel} \times LHV}{c_p (Q_{fuel} + Q_{eng})} \quad (23)$$

where LHV is the lower heating value and k_{ech} represents the amount of energy which is transferred to the exhaust pipes flow. A polynomial model of second order is used to compute this quantity for every operating point:

$$k_{ech} = f_6(N_e, Q_{fuel}, Q_{eng}) \quad (24)$$

where f_6 is a second order polynomial which coefficients are calibrated from steady state test bench data points (average

relative error is 1.8% with a standard deviation of 1.4% while maximum relative error is 6.3%).

4.11 Summary

The model is described by four differential equations. Three of them concern the pressure dynamic in the control volumes and are of the form of (7). The last one describes the turbocharger dynamic (see (17)).

For computation time consideration, the use of a discrete form is highly recommended to compute the variable at step $k+1$ from values at step k :

$$\begin{cases} P_{ape}^{k+1} = P_{ape}^k + \frac{\gamma r}{V_{ape}} (Q_{comp} \theta_{apc} - Q_{thr} \theta_{ape}) \Delta t \\ P_{man}^{k+1} = P_{man}^k + \frac{\gamma r}{V_{man}} \theta_{man} (Q_{thr} - Q_{eng}) \Delta t \\ P_{avt}^{k+1} = P_{avt}^k + \frac{\gamma r}{V_{avt}} \theta_{avt} (Q_{eng} + Q_{fuel} - Q_{turb} - Q_{wg}) \Delta t \\ \omega_t^{k+1} = \omega_t^k + \frac{1}{J} (T_{qturb} - T_{qcomp}) \Delta t \end{cases} \quad (25)$$

where V_{ape} , V_{man} and V_{avt} respectively represent the volume between the compressor and the throttle, the volume of the inlet manifold and the outlet manifold volume (see figure 2). Q_{thr} and Q_{wg} stand for the throttle and wastegate flows, both obtained with (9). Δt is the sampling time and equal to 1 ms.

5. TURBOCHARGER DATA-MAPS EXTRAPOLATION

Most turbocharger models, which can be found in literature, are based on data-maps. However, the data-maps provided by turbocharger manufacturers usually only contain few points at high iso-speeds (data points are usually only provided for iso-speeds greater than 40% of the maximum turbocharger rotational speed). That's why, in order to simulate realistic driving cycles, the information at lower rotational speeds must be extrapolated.

In this context, a new physical-based strategy of extrapolation has been developed in order to tackle the different problems induced by current methods (Jensen et al., (1991), Martin et al., (2009b), Moraal et al., (1999)). These algorithms are fully detailed and proven in El Hadeef et al., (2012).

5.1 Compressor pressure ratio

For the compressor mass flow rate (see figure 3), an analysis of the general turbo machinery equations (see El Hadeef et al., (2012)) has led to a new physics-based algorithm. It relies on the dimensionless head parameters Ψ and flow rate Φ (Martin et al., (2009a)):

$$\Psi = \frac{A(\omega_t) + B(\omega_t)\Phi}{C(\omega_t) - \Phi} \quad (26)$$

where the head parameter Ψ and the dimensionless flow rate Φ are respectively a normalisation of the pressure ratio π_{comp} and the mass flow rate Q_{comp} and A , B and C are fitted using gradient optimization algorithm on manufacturer's data points.

Using monotone piecewise cubic interpolation has demonstrated very accurate results in this case (Draper et al., (1998), Fritsch et al., (1980)).

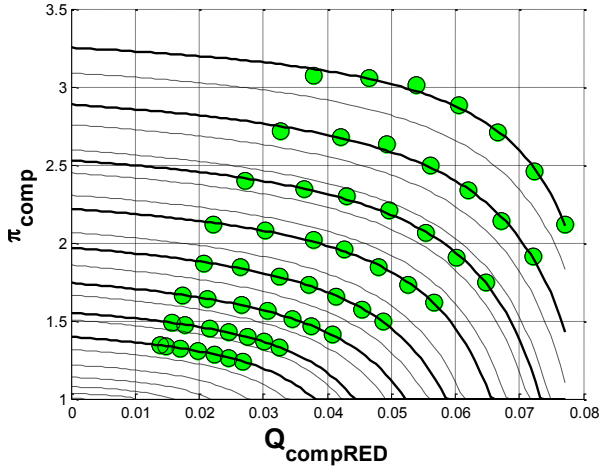


Fig. 3. Compression ratio π_{comp} versus reduced mass flow rate $Q_{compRED}$. For each supplier's iso-speed, the pressure ratio is plotted (solid lines) and compared to the manufacturer's points (white stars). New iso-speeds, interpolated and extrapolated, are also presented (dash-dot lines).

Another advantage of the model presented here is that (26) can directly be inverted to compute the exact inverted data map which is required in (11). In fact, one can easily write:

$$\Phi = \frac{C(\omega_t)\Psi - A(\omega_t)}{B(\omega_t) + \Psi} \quad (27)$$

5.2 Compressor isentropic efficiency

The isentropic efficiency of the compressor η_{comp} (see figure 4) is given by the ratio of the isentropic specific enthalpy exchange Δh_{is} and the specific enthalpy exchange Δh :

$$\eta_{comp} = \frac{\Delta h_{is}}{\Delta h} \quad (28)$$

When the head parameter has been extrapolated with (26), the isentropic specific enthalpy exchange can be directly deduced through the entire operating range:

$$\Delta h_{is} = \frac{1}{2} \Psi U_c^2 \quad (29)$$

where U_c is the blade tip speed :

$$U_c = \frac{\pi}{60} D_c \omega_t \quad (30)$$

where D_c is the wheel diameter.

One can notice that the improvements achieved on the extrapolation of the expansion ratio have a direct influence here.

For the specific enthalpy exchange, Martin has proven that it is described by a linear equation (Martin et al., (2009a), Martin et al., (2009b)), particularly adapted to be fitted:

$$\Delta h = b(\omega_t) - a(\omega_t) Q_{compRED} \quad (31)$$

where, a and b are second order polynomials fitted using gradient optimization algorithm on the manufacturer's data points and $Q_{compRED}$ is the reduced compressor flow rate (Eriksson, (2007), Eriksson et al., (2002)).

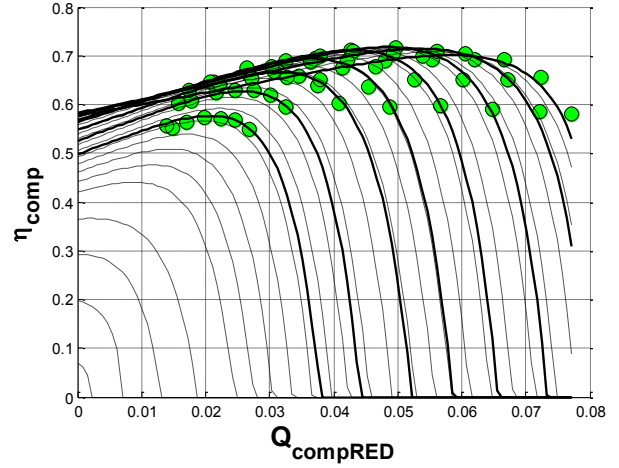


Fig. 4. Isentropic efficiency η_{comp} versus reduced mass flow rate $Q_{compRED}$. The extrapolated compressor efficiency (solid lines) well suits to the manufacturer's data points (white and black stars) through the entire flow rate range. New iso-speeds, interpolated and extrapolated, are also presented (dash-dot lines).

5.3 Turbine pressure ratio

In literature, the turbine is usually modelled as a flow restriction. Its flow rate (see figure 5) is given by the standard equations of compressible gas flow through an orifice (Moulin et al., (2008)):

$$Q_{turbRED} = S \times V_{ns} \quad (32)$$

where $Q_{turbRED}$ is the reduced turbine mass flow rate (Eriksson, (2007), Eriksson et al., (2002)), S the equivalent section and V_{ns} the reduced flow speed which depends of the flow state (subsonic or supersonic, see (9)).

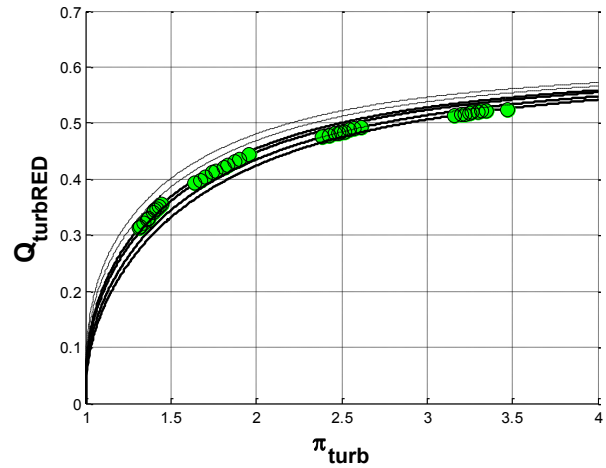


Fig. 5. Extrapolated reduced flow rate $Q_{turbRED}$ versus pressure ratio π_{turb} . For each manufacturer's iso-speed, the turbine flow rate extrapolated through the whole pressure ratio operating range is presented (solid line) as well as the reference points that have been used to fit the model (black and white stars). New iso-speeds, interpolated and extrapolated, are also presented (dash-dot lines).

The performance of such a model essentially relies on the definition that is given to the equivalent section S .

Definitions used in literature (Jensen et al., (1991), Martin et al., (2009b), Moraal et al., (1999)) usually show good performance locally (i.e. around the manufacturer's data points). However, they also suggest that the flow rate tend to infinite at high pressure ratio. This is not what is observed experimentally. In fact, from experimental observations, one can define three hypotheses for the evolution of the equivalent section with respect to the reduced mass flow rate defined in (32):

H₁: S is strictly monotonic with π_{turb}

H₂: $\lim_{p_{it} \rightarrow 1} S = 0$

H₃: $\lim_{p_{it} \rightarrow +\infty} S = constant$

According to these hypotheses, a completely new definition of S has been proposed:

$$S = k_1 \times \left(1 - e^{\left(1 - \frac{1}{\pi_{turb}}\right)^{k_2(\omega_t)}} \right) \quad (33)$$

where k_1 is a constant and k_2 a second order polynomial. Both are fitted using gradient optimization algorithm on the data provided by the manufacturer.

5.4 Turbine isentropic efficiency

The isentropic efficiency (see figure 6) is calculated in the same manner as for the compressor:

$$\eta_{turb} = \frac{\Delta h}{\Delta h_{is}} \quad (34)$$

Under the hypothesis of constant fluid density (Vitek et al., (2006)), the specific enthalpy exchange is calculated using a linear equation (Martin et al., (2009a), Martin et al., (2009b)):

$$\Delta h = c(\omega_t) Q_{turbRED} + d(\omega_t) \quad (35)$$

where c and d are second order polynomials calibrated from manufacturer's data points using regression analysis.

The isentropic specific enthalpy exchange only depends on the pressure ratio. It is computed with:

$$\Delta h_{is} = \left(1 - \left(\frac{1}{\pi_{turb}} \right)^{\frac{\gamma-1}{\gamma}} \right) C_p T_{avt} \quad (36)$$

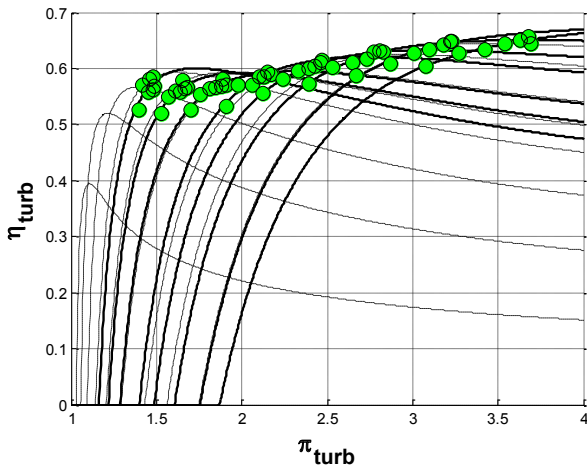


Fig. 6. Extrapolated isentropic efficiency η_{turb} . The turbine isentropic efficiency is extrapolated through the entire expansion ratio range π_{turb} (solid lines) and compared to the reference values provided in the initial data-map (white and black stars). For these iso-speeds the model well fits to the supplier's points. New iso-speeds, interpolated and extrapolated, are also presented (dash-dot lines).

6. RESULTS AND DISCUSSION

6.1 Steady-state reference simulator performances

As it is detailed in section 3, the building of the model is only based on steady state test bench operating points. The model performances for these steady state points are illustrated in figures 7 to 9.

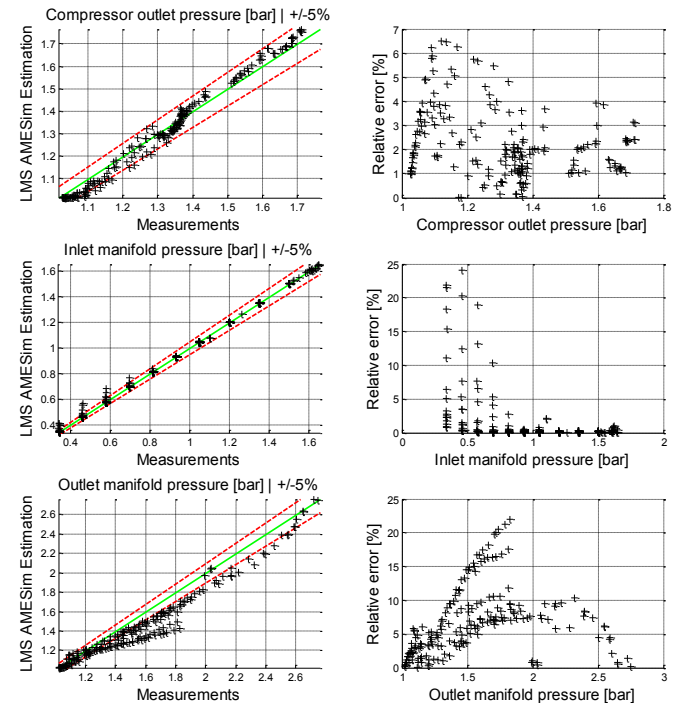


Fig. 7. Steady-states pressures validation for the reference simulator. For each physical quantity, correlation lines are plotted on the left. A perfect model would give 45 degrees tilted straight line. Dashed lines show variation zones specified in the title. Relative error versus test bench measurement is plotted on the right.

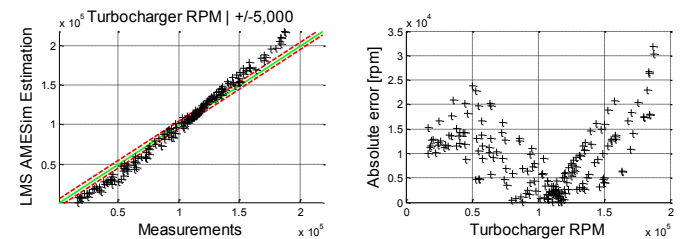


Fig. 8. Steady-states turbocharger rotational speed validation for the reference simulator.

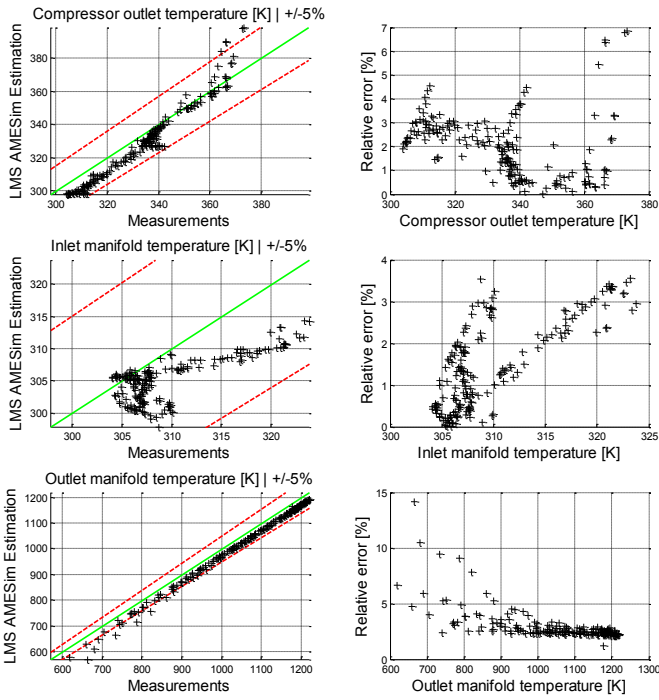


Fig. 9. Steady-states temperatures validation for the reference simulator.

6.2 Steady-state control embedded model performances

The control embedded model validation stage uses the same steady state operating points as for the reference simulator. All the results are presented in figures 10 to 12.

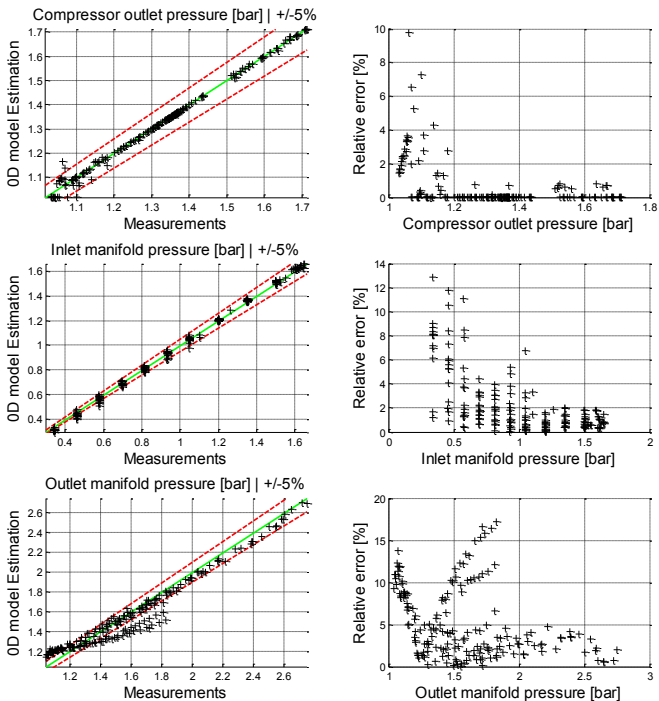


Fig. 10. Steady-states pressures validation for the control embedded model.

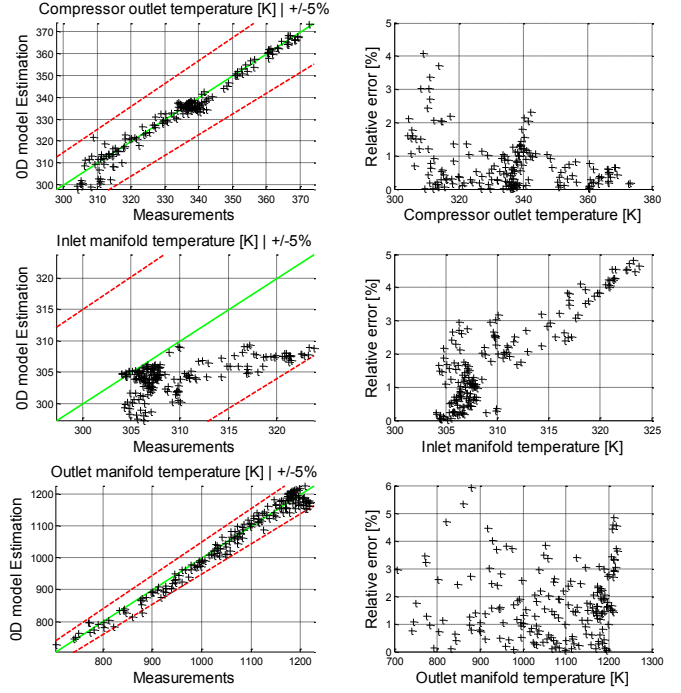


Fig. 11. Steady-states temperatures validation for the control embedded model.

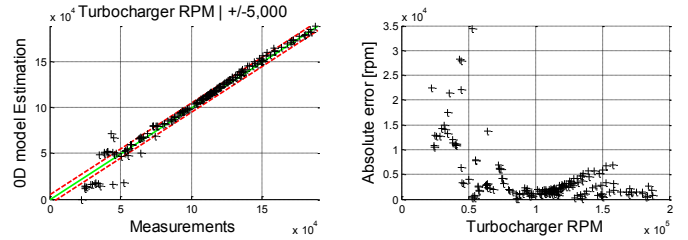


Fig. 12. Steady-states turbocharger rotational speed validation for the control embedded model.

6.3 Discussion

Both models basically have the same static behaviour. On figures 7 to 9 and on figures 10 to 12, one can see that both models present a low relative error (particularly at high loads). For pressures and temperatures, the average relative error for the AMESim model is about 10%. The average relative error on these values for the control embedded model is even lower. The estimation of the turbocharger speed is less accurate. The error can reach 30,000 rpm for the reference simulator while it reaches only 25,000 rpm for the second model at low speeds.

For control purposes, it is crucial to capture the dynamic of control variables, i.e. the pressures in the control volumes. For both models, these dynamics are well estimated (see figure 13). The relative error is less than 5% for compressor outlet and inlet manifold pressures. The performance is a bit higher for the outlet manifold pressure: the error can locally reach 20% on the transient presented here, but the dynamic is usually good. In both models, the turbocharger rotational speed dynamic is well captured (the average error is less than 9,000 rpm), in particular at low rotational speeds and pressure ratios, where the data are fully extrapolated.

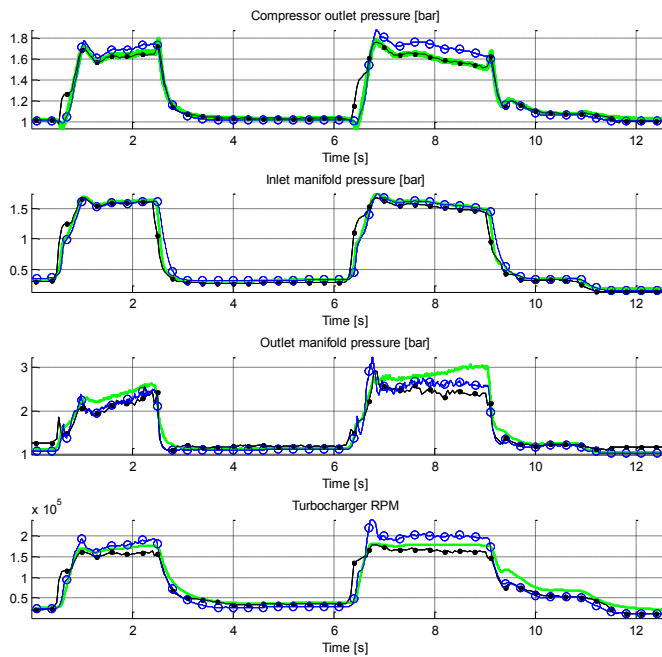


Fig. 13. Transients validation of pressures and rotational speed for the reference simulator (blue circled line) and for the control embedded model (black dotted line). Vehicle measurements are also plotted (thick light coloured line). Engine speed varies from 4,000 to 6,000 rpm while throttle and wastegate positions vary from closed to fully opened (including sudden opening).

6.4 Limitations

One should notice that the difference between the measurements and the simulation results is a global error which can be addressed to three different main sources of error: the pulse effects, the thermal effects and the extrapolation algorithms. The first two are not explicitly taken into account in the model. Moreover, the part that each phenomenon has on the error cannot be evaluated with the data presented here. That is why a comparative study between a 0D model based on a classical extrapolation method or based on the new one is irrelevant.

The goal of this study was to show that any classical control-oriented model, identified using exclusively steady states test bench measurements and based on data maps extrapolated using the new physics-based algorithms, leads to accurate enough results in the context of an industrial application.

7. CONCLUSION

Extrapolated turbocharger rotational speeds zone can easily represent 50% of a classical driving cycle. This study has been motivated by the difficulty encountered with standard techniques to obtain accurate data in this operating range. Thanks to an appropriate combination of physics and mathematical fitting tools, it has been shown that the new extrapolation strategy leads to accurate control-oriented engine models. The advantage is that the new algorithms are more robust than standard methods while keeping the zero dimensional approach and a low CPU load requirement.

REFERENCES

- Chauvin, J., Grondin, O., and Moulin, P. (2011). Control Oriented Model of a Variable Geometry Turbocharger in an Engine with Two EGR loops. *Oil & Gas Science and Technology - Rev. IFP Energies nouvelles*, 66 (4), 563-571.
- Dauron, A. (2007). Model-Based Powertrain control: Many Uses, No Abuse. *Oil & Gas Science and Technology - Rev. IFP Energies nouvelles*, 62 (4), 427-435.
- Draper, N. R., and Smith, H. (1998). *Applied Regression Analysis*. Wiley.
- El Hadej, J., Colin, G., Talon, V., and Chamailard, Y. (2012). Physical-Based Algorithms for Interpolation and Extrapolation of Turbocharger Data Maps. *SAE Int.J.Engines 5(2):2012*, doi:10.4271/2012-01-0434
- Eriksson, L. (2007). Modeling and Control of Turbocharged SI and DI Engines. *Oil & Gas Science and Technology - Rev. IFP Energies nouvelles*, 62 (4), 523-538.
- Eriksson, L., Nielsen, L., Brugard, J., and Bergström, J. (2002). Modeling of a Turbocharged SI Engine. *Annual Reviews in Control*, 26, 129-137.
- Fritsch, F. N., and Carlons, R. E. (1980). Monotone Piecewise Cubic Interpolation. *SIAM Journal on Numerical Analysis*, 17 (7).
- Gissinger, G., and Le Fort-Piat, N. (2002). *Contrôle Commande de la Voiture*. Hermès Lavoisier.
- Guzzella, L., and Onder, C. H. (2004). *Introduction to Modeling and Control of Internal Combustion Engine Systems*. Springer.
- Hendricks, E. (2001). Isothermal versus Adiabatic Mean Value SI Engine Models. *3rd IFAC Workshop, Advances in Automotive Control*, 373-378.
- Heywood, J. B. (1988). *Internal Combustion Engines Fundamentals*. McGraw-Hill.
- Jensen, J.-P., Kristensen, A. F., Sorenson, S. C., Houbak, N., and Hendricks, E. (1991). Mean Value Modeling of a Small Turbocharged Diesel Engine. *SAE Technical Paper*, 910070.
- Martin, G., Talon, V., Higelin, P., Charlet, A., and Cailloil, C. (2009a). Implementing Turbomachinery Physics into Data-Map Based Turbocharger Models. *SAE Technical Paper*, 2009-01-0310.
- Martin, G., Talon, V., Peuchant, T., Higelin, P., and Charlet, A. (2009b). Physics Based Diesel Turbocharger Model for Control Purposes. *SAE Technical Paper*, 2009-24-0123.
- Moraal, P., and Kolmanovsky, I. (1999). Turbocharger Modeling for Automotive Control Applications. *SAE*, 1999-01-0908.
- Moulin, P., Chauvin, J., and Youssef, B. (2008). Modelling and Control of the Air System of a Turbocharged Gasoline Engine. *Proc. of the IFAC World Conference 2008*.
- Talon, V. (2004). *Modélisation 0-1D des Moteurs à Allumage Commandé*. PhD Thesis, Université d'Orléans.
- Vitek, O., Macek, J., and Polasek, M. (2006). New Approach to Turbocharger Optimization using 1-D Simulation Tools. *SAE Technical Paper*, 2006-01-0438.